FRONTIERS ARTICLE

Mechanisms for S–S and N–C$_\alpha$ bond cleavage in peptide ECD and ETD mass spectrometry

Jack Simons

Chemistry Department, Henry Eyring Center for Theoretical Chemistry, University of Utah, Salt Lake City, UT 84112, United States

ARTICLE INFO

ABSTRACT

This Letter reviews efforts made to elucidate the mechanism by which electron-capture and electron-transfer dissociation bond cleavages occur in mass spectrometry. The primary issues include where in the parent ion the electron initially attaches, whether the energy released in this initial electron-capture step is key to determining which bonds will cleave, whether the electron can migrate from the site to which it initially attaches to other sites in the parent ion, and, if so, over what distances and at what rates, and why, in polypeptides, one finds disulfide and N–C$_\alpha$ bond cleavage primarily.

© 2009 Published by Elsevier B.V.

1. Introduction

This Letter overviews efforts to gain understanding of how electrons induce very specific bond cleavages when they attach to gas-phase peptides having one or more positively charged groups in mass spectrometry experiments. In electron-capture dissociation [1–4] (ECD) experiments, one subjects a mass-to-charge-selected parent ion to very low-energy electrons (often boiled off a filament) and then monitors the identities and abundances of the fragment ions generated subsequent to electron capture. In electron-transfer dissociation [5–9] (ETD), one allows the parent ion to undergo collisions with an anion donor having low electron binding energy, which transfers an electron to the parent to produce the fragment ions. Both experiments are usually carried out at or near room temperature. As a result, in ECD the primary source of excess energy is the recombination energy released when the electron is captured, while, in ETD, this recombination energy is reduced by the electron binding energy of the anion donor.

The work discussed here is important because ECD and ETD have shown much utility and promise for sequencing peptides and proteins. Both methods selectively cleave disulfide and N–C$_\alpha$ bonds and do so over a wide range of the peptide backbone, thus producing many different fragment ions. This is unlike collision-induced dissociation (CID) or infrared multi-photon dissociation (IRMPD), in which fewer distinct fragment ions are usually formed. ECD and ETD also preserve labile side-chains with post-translational modifications, which is another positive attribute. However, the precise mechanism(s) by which the ECD or ETD attached electron induces the bond cleavages needs to be better understood to optimize the utility of these techniques.

Parallel with many advances in the experimental development and improvement of these methods, theoretical studies have been carried out by several groups to try to determine the mechanism(s) [10–36] by which electron attachment leads to these specific bond cleavages as well as how the initial electron attachment occurs.

In Fig. 1, we show a qualitative depiction of a multiply charged polypeptide with one peptide bond labeled and one N–C$_\alpha$ and disulfide linkage also identified. Also shown is an anion donor CH$_3^-$ approaching this peptide (as in ETD), and several distances between various sites in the peptide and donor are labeled for future reference.

Fig. 1 is useful for introducing several key questions that have been the focus of experimental and theoretical studies on the mechanism(s) of ECD and ETD including:

1. At what sites in the gas-phase multiply charged polypeptide can the ECD or ETD electron attach? Being negative, won't electrons and anion donors be attracted to the positive sites and thus more likely to deposit an electron there? Are some positive sites favored over others?
2. It is known that (i) electrons can be captured into Rydberg orbitals on positive groups such as protonated amines and (ii) the energy released (the so-called recombination energy RE) in such capture events can be substantial (e.g., ca. 4 eV for capture by a protonated amine). If an ECD or ETD electron is attached to a positive site, is the RE the source of the energy used to cleave the SS and N–C$_\alpha$ bonds?
3. Why do N–C$_\alpha$ bonds rather then the somewhat weaker peptide bonds cleave under ECD and ETD, whereas the opposite occurs under CID and IRMPD?
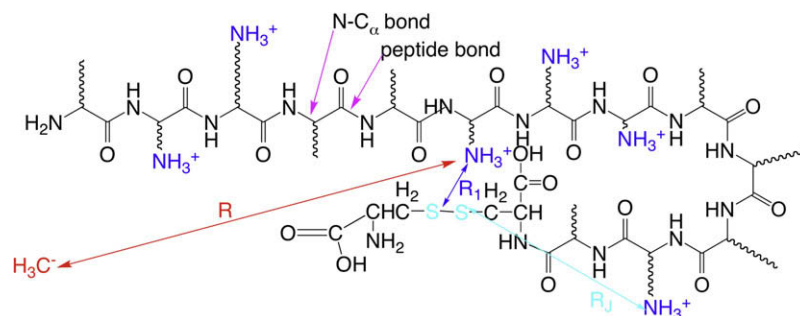
Fig. 1. Sketch of a typical multiply positively charged polypeptide with several of its side chains (wavy lines) protonated. Also labeled are one SS bond, one peptide bond, and one N–C$_\alpha$ bond as well as some distances from the SS bond to positive sites. Also shown is an anion donor (H$_3$C$^-$) a distance R from the polypeptide.

4. Can an electron be captured directly at the disulfide or N–C$_\alpha$ bond site? If so, how and under what conditions?

5. After electron attachment to one site occurs, can the electron subsequently migrate to other site(s)? If so, over what distance is migration feasible and between what pairs of sites?

6. What is the molecular-level mechanism by which the attached electron induces the disulfide or N–C$_\alpha$ bond cleavage observed in ECD/ETD experiments?

2. Historical overview

2.1. The Cornell mechanism

Let us now overview the history of experimental and theoretical findings that guided our work since we entered the field [19] in 2003. In the earliest experimental work on ECD [1–4], it was postulated by the McLafferty group that electrons were initially captured at a positively charged site to form a Rydberg (a.k.a. hypervalent) radical center (e.g., one of the –NH$_3$ centers in Fig. 1) with an accompanying substantial (ca. 4 eV for forming –NH$_3$ from $-NH_3^+ + e^-$) release of energy. Although the initial electron capture could populate an excited Rydberg level, it was known that such excited states undergo a series of relaxations (radiative or radiationless) at rates of ca. $10^6\,s^{-1}$ to populate lower Rydberg states, eventually reaching the ground state. Further, based on earlier work on such dissociative recombination (DR) processes, it was posited that, once the ground Rydberg level is reached, the nascent hypervalent species could eject or release an H atom which could then attack either (i) an S–S bond to cleave it (forming an –S· radical and a HS– molecule) or (ii) a backbone carbonyl oxygen atom to form a –(·COH)–NH–C$_\alpha$– radical center. In the latter case, the –(·COH)–NH–C$_\alpha$– radical would then have a much-reduced barrier to cleaving its N–C$_\alpha$ bond because a C–N π bond could be formed as the N–C$_\alpha$ bond is broken. This earliest mechanistic proposal, commonly called the Cornell mechanism, is described in Scheme 1.

This well-founded conjecture was based on knowledge that

(i) Positively charged closed-shell molecules could attach an electron to form a hypervalent species in which the attached electron occupies a Rydberg orbital on the charged site.

(ii) The attached electron might enter the lowest Rydberg orbital or any of a myriad of excited Rydberg orbitals.

(iii) An electron in an excited Rydberg orbital most likely undergoes a series of radiative or radiationless transitions (occurring over several microseconds) to lower Rydberg states.

(iv) Once the electron reaches the lowest (or one of the lowest few) Rydberg states, dissociation occurs; for –NH$_3$ species, either an H atom is promptly (in ca. 10^{-9} s) ejected (to leave –NH$_2$) or an NH$_3$ molecule is released, thus terminating the dissociative recombination event.
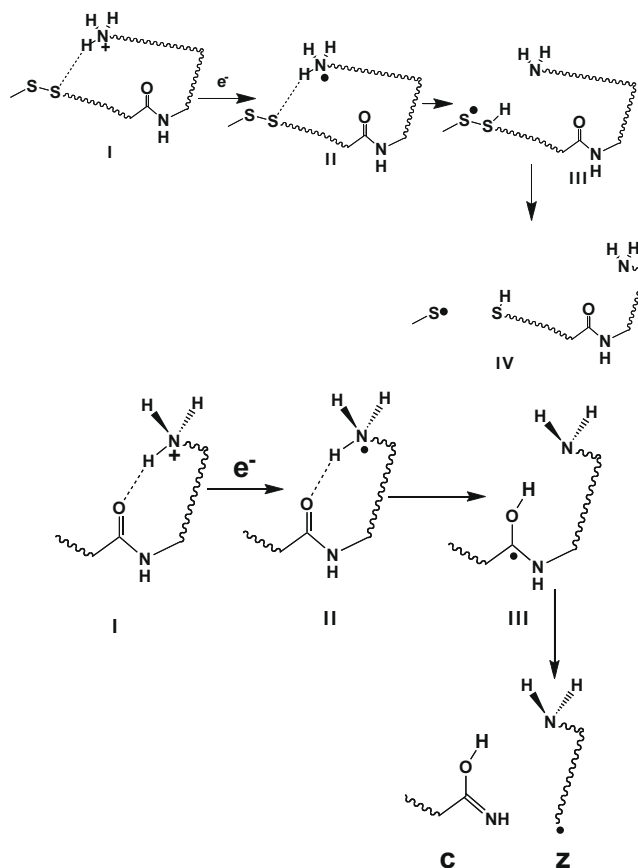
Scheme 1. The original Cornell mechanism for H atom release from Rydberg sites to cleave disulfide or N–C$_\alpha$ bonds. Note also the c and z notation used to label the fragments obtained when a N–C$_\alpha$ bond cleaves.

In the Cornell mechanism, dissociative recombination (which, as noted earlier, can be exothermic by up to ca. 4 eV) can lead to free H atoms. These atoms, in turn, were proposed to either add to S–S bonds or amide carbonyl bonds, to thus induce the observed ECD bond cleavages. Note that this mechanism indeed rationalizes why (stronger) N–C$_\alpha$ bonds rather than (weaker) peptide bonds are cleaved, and it is based on solid knowledge from the spectroscopy community about the behavior of molecular Rydberg states. Also note that, most samples used in ECD and ETD under analytical conditions have a large number of positive charges, many of which are expected to involve protonated basic side chains. Such protonated sites, in turn, are expected to be involved in hydrogen bonds to nearby carbonyl oxygen or disulfide sulfur atoms. Thus, is makes sense that hydrogen atoms liberated via dissociative
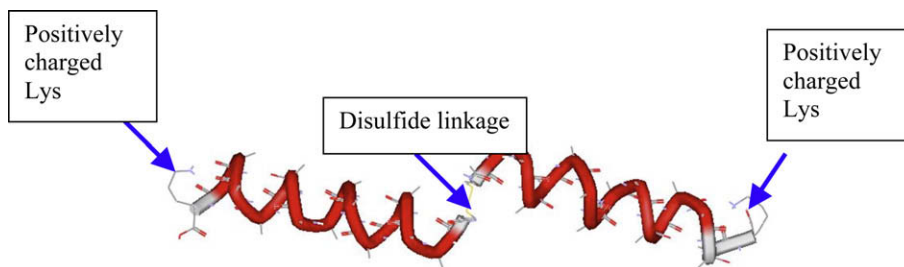
Fig. 2. Assumed structure of doubly charged $(AcCA_{1}5K + H)_{2}^{2+}$ cations in gas phase (redrawn from Ref. [19]).

recombination at such sites could access and attach to S–S or amide C=O bonds as proposed.

2.2. Evidence that H atoms may not be necessary

In 2002, experimental results from the Marshall lab [37] provided data suggesting that the H atom mechanism just discussed may not be correct, or at least, may not be the only mechanism for cleaving SS and N–C_α bonds under ECD conditions. In Fig. 2, we show a doubly positively charged polypeptide containing a disulfide linkage at its center, two alanine helices on its right and left, and two terminal protonated lysines at the C-termini. This is the parent ion that the Marshall group subjected to ECD and found

(i) strong abundance (60–75% of the backbone cleavage) of fragment ions resulting from cleavage of the S–S bond and having mass consistent with formation of the –S· radical plus a charge-reduced neutral fragment,

(ii) fragment ions consistent with significant cleavage of N–C_α bonds within the four Ala units closest to the Lys termini but no N–C_α cleavage further from the Lys termini,

(iii) very similar fragment ion yields, regardless of whether 15 (as in Fig. 2), 10, or 20 Ala units were in the two helical units, and

(iv) similar fragment ion yields even when the protonated Lys termini were replaced by positively charged Lys termini with Na^+ cations providing the charge (i.e., –$LysNa^+$).

The Marshall group's data conflicts with the Cornell mechanism because:

(i) Although H atoms released via DR from the Lys sites could be close enough to the four Ala units nearest the Lys termini to effect N–C_α cleavage at these Ala sites, it is difficult to understand how these H atoms can (with high probability as required by the disulfide yields quoted above) travel up to 32 Å (for $(AcCA_{20}K + H)_{2}^{2+}$) to attack and cleave the S–S bond.

(ii) Although H atoms are known to attack and cleave S–S bonds, neutral Na atoms (which would be released upon DR of –NH_2Na^+ sites) are not. Nevertheless, S-S bond cleavage occurs when the protonated Lys units are replaced by –$LysNa^+$ charged sites.

These findings on the species shown in Fig. 2 caused this author to consider two alternatives to the Cornell mechanism:

i. One in which the ECD electron is captured directly[1] into an S–S σ^* or amide π^* orbital to (promptly) cleave the disulfide linkage and form –S· and $^-$S– fragments or to form
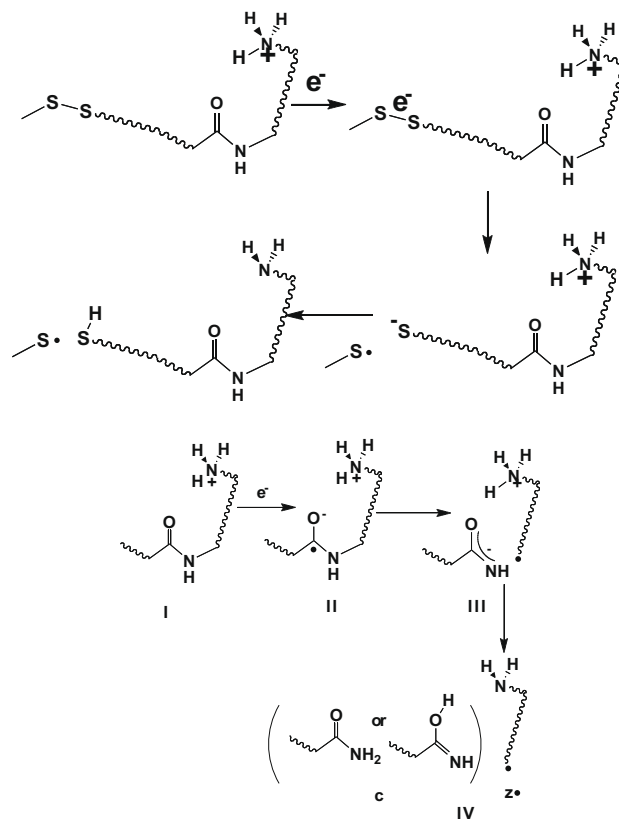
Scheme 2. Direct electron attachment to an S–S σ^* or OCN π^* orbital to cleave a disulfide or N–C_α bond.

a –(·CO^-)–NH–C_α– radical anion that then cleaves its N–C_α bond to form the p-delocalized –$^-$OC=NH anion and a carbon-based radical ·C_α–, respectively.

ii. Another in which the electron initially is captured into a Rydberg orbital at a positively charged site, and subsequently (during the relaxation cascade from excited Rydberg levels to lower levels but *before* the dissociative ground Rydberg level is reached) undergoes intra-molecular electron transfer to S–S σ^* or amide π^* orbital to effect the disulfide or N–C_a cleavage as discussed in (i). This mechanism, which is now often called the Utah–Washington mechanism, is depicted in Scheme 2 for both bond cleavage cases, as it would take place for option (i) above.

In either option (i) or (ii), intra-molecular proton transfer to the $^-$S- or –$^-$OC=NH anionic site could also, occur as a result of which one could generate the same products as in the Cornell mechanism. For N–C_α cleavage, two possible structures for the c-type fragments are shown in Scheme 2; they have identical mass-to-charge ratios,

---

so the mass spectrometry experiment cannot distinguish them. The $O=C-NH_2$ amide structure (left) is thermodynamically more stable, but, depending whether a proton is transferred from elsewhere in the polypeptide before or after the $N-C_\alpha$ bond cleaves, one would expect either the enol-imine (right) or the amide (left) to be formed, respectively. Recently, an infrared multi-photon action spectroscopic probe [38] of the c-type fragments (see Scheme 1) formed in ECD was carried out and it was determined that the amide structure is formed, not the enol-imine. However, the authors of Ref. [38] point out that it is possible the amide structure could be formed by isomerization of the initially-formed enol-imine species (i.e., there is enough energy available to effect this isomerization). So, this spectroscopic data provides evidence suggesting (but not proving) that the proton transfer takes place after the $N-C_\alpha$ bond has cleaved, not before.

2.3. Coulomb stabilization

This author was aware that it does not make sense to postulate that a low-energy (ca. 0.3 eV or less) free electron such as used in ECD could directly attach to either an S–S σ^* or an amide π^* orbital. Earlier work on dissociative electron attachment [39,40] showed that vertical electron attachment to an S–S σ^* or amide π^* orbital is ca. 1 eV or ca. 2.5 eV *endothermic*, respectively. However, we suggested that these low-lying anti-bonding orbitals can have their energies[2] lowered by their attractive Coulomb interactions with positively charged groups (e.g., the protonated amine or fixed-charge groups on side chains) thus rendering *exothermic* electron attachment to these orbitals (either directly or via transfer from a positive site). A disulfide linkage must experience Coulomb stabilization exceeding 1 eV for ECD to render our this mechanism feasible; this stabilization could arise, for example, from a single positively charged site closer than ca. 14 Å, from two positive sites each 28 Å distant, or from a doubly charged site 28 Å away. Analogously, we postulated that a single positive charge 14.4/2.5 = ca. 6 Å from an OCN π^* orbital could render this orbital amenable to exothermic electron attachment because such orbitals need to be Coulomb stabilized by ca. 2.5 eV. Of course, in a multiply charged polypeptide, all of the Coulomb potentials contribute to this stabilization of each SS and amide site, suggesting that it might be possible for many of the SS σ^* or amide π^* orbitals to attach an ECD electron (either directly or via transfer from a positive site's Rydberg orbital).

In a very large peptide or protein, some intra-molecular dielectric screening can occur thus reducing the Coulomb potential. However, the screening will be much less than in the bulk because, to realize full screening, one needs the charges to be *surrounded by* a dielectric not just have dielectric separating them. For example, Prof. Lai-Sheng Wang's group has studied [41] photoelectron spectra of dicarboxylate dianions $^-OOC-(CH_2)_n-COO^-$ and found the electron detachment (DE) energies of such species can be fit to DE = $(3.21 - 16.7/R_Å)$ eV, where 3.21 eV is the intrinsic DE of an individual carboxylate anion in the absence of any Coulomb potential from the other site, and $R_Å$ is the distance between the two carboxylate sites. The -16.7 slope of Ref. [41]'s plot of DE vs. $1/R_Å$ is close to the unscreened -14.4 slope. If the aliphatic $-(CH_2)_n-$ spacers provided screening, one would expect a slope closer to $-14.4/2$, given that aliphatic hydrocarbons have dielectric constants near 2.

Up until this stage in our studies, the evidence seemed to point to

(i) either the Cornell mechanism being incorrect or not being the only pathway by which SS and $N-C_\alpha$ bonds are cleaved in ECD,

(ii) the possibilities that ECD electrons could attach directly to SS σ^* or amide π^* orbitals and thus cause the bond cleavages observed in ECD, or

(iii) that ECD electrons could attach to positively charged sites and subsequently undergo some form of inter-molecular transfer to an SS σ^* or amide π^* orbital to effect the bond cleavage.

So, in some of our earliest studies, as we now discuss, we attempted to address the question of where the ECD electron attaches – to SS σ^* or amide π^* orbital or to a Rydberg orbital on a positively charged site.

2.4. Where is the electron most likely to attach?

Because both the ECD electron and the ETD anion donor are negatively charged, it is obvious that Coulomb potentials will play a key role in determining the energy landscapes pertinent to the ETD or ECD electron attachment process. They will accelerate the electron or donor anion toward the polypeptide, and they will Coulomb-stabilize the SS σ^* and amide π^* orbitals within the peptide. Let us first consider how the energy landscape is expected to look in the ETD case[3] accompanying the collision of an anion donor (e.g., the methyl anion in Fig. 1) and a multiply positively charge polypeptide.

In Fig. 3, we show qualitative depictions of a few of the electronic states relating to the electron transfer event as functions of the distance R between the anion donor and the polypeptide having a total charge Z.

The rapidly descending red curve describes how the energy of the ion-pair state corresponding to H_3C^- and the Z-charged peptide varies with R; it follows the attractive Coulomb form $-14.4Z$ eV/ R(Å) at large-R. The other curves are meant to show the R-dependences of states in which an electron has been transferred from the H_3C^- anion donor to either (i) ground (3s) or (ii) excited (3p, 3d, 4s, 4p, etc.) Rydberg orbitals localized on one[4] of the peptide's positive sites, (iii) an SS σ^* orbital, or (iv) one of the peptide's OCN π^* orbitals. All of these states' energy profiles are shown as being rather independent of R (at least at large-R) because they relate to interactions of a neutral H_3C radical with a peptide having charge ($Z - 1$). Of course, at shorter R-values, valence-range interactions set in and cause all of these curves to eventually become repulsive, but we do not show the small-R character of the energy surfaces.

The large-R energies of the OCN π^* and SS σ^* attached states relative to that of the parent peptide of charge Z are determined by the intrinsic energies of these two orbitals (2.5 eV endothermic for the former, 1 eV for the latter) stabilized by the total Coulomb potential that each orbital experiences from all the positive sites

$$C = -14.4 \text{ eV} \sum_{J=1}^{N} \frac{Z_J}{R_J \text{ (Å)}}. \tag{1}$$

---

[2] Actually, it is the energies of the electron-attached states in which an electron occupies the SS σ^* or amide π^* orbital that are lowered. The Coulomb potential C can be written in eV as $C = 14.4$ eV Å/R(Å), when the distance is expressed in Å.

[3] We think the ECD case can be viewed as being essentially identical to ETD except that the electron binding energy of the anion donor can be taken as zero for the free electron. This is not an obviously correct assumption given the fact that low-energy free electrons have long de Broglie wavelengths and probably should be treated using quantum scattering theory. However, data that we discuss later showing that the fragmentation ion distributions observed in ETD are essentially the same as in ECD suggest that even the initial electron capture events for the two cases are governed by similar physics.

[4] In Ref. [30], it is shown that electron attachment to species with more than one positively charged site might generate Rydberg states consisting of superpositions of orbitals localized on two or more of the charged centers (i.e., the X and A state-orbitals in Fig. 4 of Ref. [30]). Because such states are close in energy (i.e., they differ by only 0.17 eV for the case shown in Fig. 4 of Ref. [30]), an ETD or ECD initial electron attachment event can be expected to populate either or both of these states.

Fig. 3. Qualitative depiction of the energies (as functions of the anion-peptide separation R) of the ion-pair state (red), states in which an electron has transferred from the anion donor to a Rydberg (ground 3s or excited 3p, 3d, 4s, 4p, etc.) orbital located on a positive site, and states in which the electron has transferred from the donor anion to an OCN π^* or SS σ^* orbital.

Here, Z_J is the charge on the Jth charged site and R_J is the distance (in Å) from that Jth site to the SS or OCN site whose Coulomb stabilization one is evaluating. Likewise, the energy of each of the Rydberg-attached states will depend on the intrinsic electron binding energy for that state (e.g., ca. 4 eV exothermic for $-NH_3^+$ sites and ca. 3 eV for $-N(CH_3)_3^+$ sites) stabilized further by the Coulomb potential at that Rydberg site due to all of the $N - 1$ *other* charged sites in the polypeptide. Clearly, as the polypeptide undergoes thermal intra-molecular motions, these Coulomb potentials will vary and, as a result, the locations of the crossings between the ion-pair state's potential and the potentials of the SS σ^*-, OCN π^*-, or Rydberg-attached states will vary with time.

In the phase of our work [17,18,22] aimed at addressing where an ETD or ECD electron is most likely to *initially* attach to a positively charged polypeptide, we carried out classical trajectory calculations (with a range of initial conditions representative of a gas-phase collision of a translationally cold anion donor with a charged peptide). Each such trajectory should be viewed as beginning on the red ion-pair state in Fig. 3. As a trajectory progressed and the two oppositely charged ions accelerated toward one another, we monitored the energies of any nearby electronic states (i.e., the Rydberg, SS σ^*, and OCN π^* states) to be aware of any surface crossing[5] that arise. Once the trajectory reached a region of surface crossing, we carried out a series of ab initio electronic structure calculations (at a finely spaced set of geometries so we could evaluate the slopes F_1 and F_2 of the two curves as well as their energy separation $2H_{1,2}$) for the energies of these two states. We then used Landau–Zener (LZ) theory to estimate the probabilities P

$$P = 1 - \exp\left[-\frac{2\pi H_{1,2}^2}{\hbar\nu|\Delta F|}\right] \approx \frac{2\pi H_{1,2}^2}{\hbar\nu|\Delta F|} \qquad (2)$$

for hopping from the ion-pair state to the other state. In Eq. (2), ν is the rate of change of the distance R between the anion donor and the site to which the electron is transferred and DF is the difference in the slopes of the two state's energy surfaces. From these LZ estimates of the surface hopping probabilities P, we were able to estimate the cross-sections s for each electron-transfer reaction

$$\sigma = 2P(1 - P)\pi R_C^2, \qquad (3)$$

where R_C is the distance between the anion donor and the site to which the electron is transferred at the crossing point of the two energy surfaces.

The main conclusions from these studies of surface hopping accompanying collisions between anion donors and positively charged polypeptides were:

(i) In the overwhelming majority of the collisions, the anion donor is closer to a positive site than to an SS or amide bond site when the surface crossing is experienced. This is not surprising given that the strong Coulomb potentials cause the donor anion to be accelerated toward the positive sites.

(ii) The surface hopping probabilities and related cross-sections are 10–100 times larger for electron transfer to a Rydberg orbital (excited or ground) on a positive site than for transfer to an SS σ^* or amide π^* orbital. The primary factor in determining these relative magnitudes is the coupling strength $H_{1,2}$ between the ion-pair and orbital states; it is much larger for the Rydberg orbitals than for the σ^* or π^* orbitals because the ion-pair collision brings the anion donor much closer to the Rydberg site than to the SS or OCN bond sites.

(iii) The cross-sections for transfer to a Rydberg orbital are substantial – often ca. 1–50 Å^2.

(iv) The cross-sections for transfer to the ground (3s) or low-energy (3p, 3d, 4s, 4p) Rydberg orbital are similar to one another. We attempted [42] to estimate hopping probabilities and cross-sections for higher Rydberg levels, but found it difficult to extract reliable $H_{1,2}$ matrix elements for states with principal quantum number $n > 4$.

So, it appears that the initial electron attachment in ETD most likely occurs into a Rydberg orbital on a positive site, but in ca. 1–10 % of the collisions, transfer to a σ^* or π^* orbital is feasible (as long at the orbital has sufficient Coulomb stabilization). For that (small) fraction of events involving direct attachment to a σ^* or π^* orbital, cleavage of the SS or N–C$_\alpha$ is expected. For the majority of events, one is faced with explaining why it is that ETD and ECD produce considerable (often dominant) S–S and N–C$_\alpha$ bond cleavage even though one expects electrons captured into Rydberg orbitals at positive sites would, after relaxation to the lower-energy Rydberg orbitals, eject H atoms or NH$_3$ molecules, as discussed earlier. Indeed, such H and NH$_3$ loss is observed, but cleavage of SS and N–C$_\alpha$ bonds throughout much of the peptide's backbone also takes place and often dominates.

These findings thus suggested that, subsequent to electron attachment into an excited Rydberg orbital but before the Rydberg electron has time to completely relax to the ground Rydberg state (recall from earlier, this is ca. 10^{-6} s), electron transfer from the Rydberg site to an SS σ^* or OCN π^* orbital may take place. This would then allow the SS or N–C$_\alpha$ bond to cleave as in Scheme 2. So, the next phase of our studies involved characterizing the rates

---

[5] Adiabatic energy surfaces do not cross but undergo a so-called avoided crossing in which they come within $2H_{1,2}$ of one another. It is common to speak of surface hopping when curves cross and we will retain this language. However, it is the diabatic curves that cross, not the adiabatic curves that we generate in our ab initio calculations.

of such Rydberg-to-valence (σ^* or π^*) electron transfer events and determining the distances over which such transfer can occur. It also involved determining whether it matters which excited Rydberg state is populated in the initial electron attachment event and determining whether electron transfer from a Rydberg orbital on one positively charged site to a Rydberg orbital on another site could take place.

2.5. Rydberg-to- σ^* or π^* electron transfer

First, let us deal with the issue of whether it matters which excited Rydberg state is populated in the initial ECD or ETD event. Clearly, on the basis of energy considerations alone, a free electron (as in ECD) can be attached to the ground or *any* excited Rydberg state on any positive site. However, an ETD electron cannot access as high-energy Rydberg orbitals as in ECD because the anion donor's electron binding energy must be overcome to conserve energy in the transfer process. Nevertheless, the peptide fragmentation patterns found in ETD and ECD are found to be extremely similar. Moreover, even in electron-capture-induced dissociation [43] (ECID), where an electron is transferred to the polypeptide in a collision with ground-state sodium ($3s^1$; ^2S) or cesium ($6s^1$; ^2S) atoms and where even greater limitations exist on which Rydberg states can be accessed, the fragmentation patterns are also quite similar. These nearly identical fragmentation propensities suggest that (i) initial population of high-energy Rydberg states or (ii) electron transfer from such high-energy states (to σ^* or π^* orbitals) may not be essential in determining product-ion yields. In fact, we think these data suggest that (i) ECD, ETD, and ECID may indeed initially populate different distributions of Rydberg states, but (ii) as these Rydberg states undergo relaxation to lower levels, it is the lower-energy Rydberg states that are most effective in transferring the electron to an SS or amide site. In recent work [42], we showed theoretical evidence suggesting that excited Rydberg states with principal quantum number $n < 10$ are more central to the electron transfer mechanisms that we now discuss.

2.5.1. Results from ab initio electronic structure calculations

To address the possibility of electron transfer [25–27] from a Rydberg orbital on a positive site to a Coulomb-stabilized SS σ^* or amide π^* orbital, we carried out a series of ab initio calculations within which we elongate the bond to be broken (i.e., the SS or N–C_α bond) and we look for curve crossings between (i) an excited Rydberg state and (ii) the state in which the electron occupies either the SS σ^* or amide π^* orbital. At each avoided crossing, we extract the $H_{1,2}$ values that relate to the coupling between the Rydberg-attached and valence-attached states. To illustrate, we show in Fig. 4 the energy profiles for a small model compound containing one protonated amine site and one disulfide bond.

For the compound whose curves are shown in Fig. 4, the charged site experiences no Coulomb stabilisation, whereas the SS site is stabilized by its interaction with the protonated amine ca. 3.5 Å away. The intrinsic electron binding energy of the ·S–CH_3 radical (ca. 2 eV), stabilized by its Coulomb interaction (14.4/3.5 = 4 eV) thus causes the energy of the σ^*-attached state to lie 6 eV below the parent at large-R as shown in Fig. 4. When viewed as a model for an SS bond and a charged site in a polypeptide, it is important to realize that the relative energies of the σ^*-attached and Rydberg-attached curves may shift somewhat due to the differential Coulomb stabilization energies at the SS and charged sites, but their general shapes as functions of R are expected to be much as shown in Fig. 4.

Clearly, there are many Rydberg levels that undergo avoided crossings with the SS σ^*-attached state. Which levels cross depends upon (i) the recombination energies associated with the particular positive site (in Fig. 4, it is a protonated amine) and (ii) the
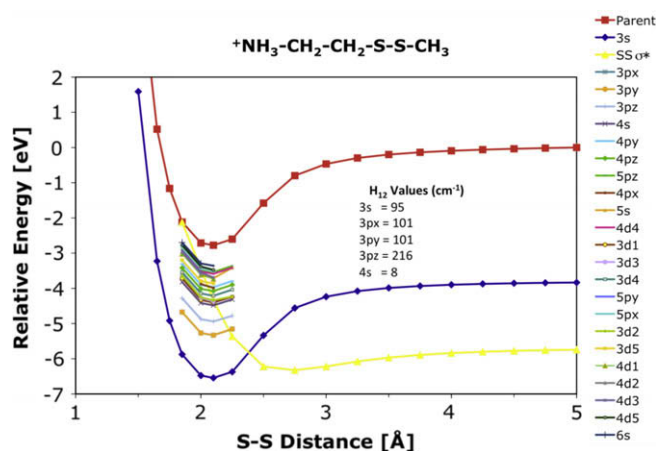
Fig. 4. Energies of the parent cation (red), ground 3s Rydberg-attached (blue), and SS σ^*- attached (yellow) states of a model compound containing an aliphatic linkage between protonated amine and disulfide bond sites, as functions of the SS bond length Also shown are energies of 3p, 3d, 4s, 4p, 4d, 5s, and 5p Rydberg-attached states and the $H_{1,2}$ coupling matrix elements between the SS σ^* and 3s, 3p, and 4s Rydberg states (taken from Ref. [45]).

total Coulomb stabilization energy experienced by the SS σ^* orbital (in Fig. 4 it is only the potential from the one protonated amine). Therefore, exactly which Rydberg states cross the SS σ^* state will vary from system to system. However, it is crossings occurring near the equilibrium SS bond length (R_e) that are most important because the internal temperature of the gaseous polypeptide is near room temperature even though the exothermicity (as high as ca. 4 eV) of the electron capture event is considerable. It is thought that this recombination energy is redistributed among the many internal vibrational modes of the polypeptide, so there is little chance that much of this excess energy resides in the S–S bond-stretching coordinate. Thus, for the system shown in Fig. 4, it is the $n = 4$ and higher Rydberg states that need to be considered; the $n = 3$ Rydberg states do not cross the σ^*-attached state near R_e.

By carrying out calculations on several such model compounds (e.g., ^+H_3N–$(CH_2)_k$–S–S–CH_3 with various k) and extracting $H_{1,2}$ coupling strengths from the myriad of avoided crossings that occur, we came to certain conclusions. The first is that, for a given Rydberg state (e.g., 3s, 3p, 3d, 4s, etc.), the $H_{1,2}$ couplings appear to decay exponentially with the distance R between the center of the Rydberg orbital and the location of the bond being cleaved (SS or N–C_α). These trends are illustrated in Fig. 5 where data for the 3s and 3p Rydberg states of ^+H_3N–$(CH_2)_k$–S–S–CH_3 are plotted and the SS σ^*, 3p, and 3s Rydberg orbitals are shown (to emphasize to what extent and over what distances these orbitals can overlap).

Based upon the $H_{1,2}$ values (and slopes) obtained for the Rydberg-to-valence (SS σ^*) curve crossings in these model compounds, we were able to again use Landau–Zener theory to estimate the rate of electron transfer

$$Rate = 1.8 \times 10^{13} \left\{ 1 - \exp\left[-\frac{2\pi H_{1,2}^2}{\hbar v |\Delta F|} \right] \right\} \text{ s}^{-1}$$

$$\approx 1.8 \times 10^{13} \frac{2\pi H_{1,2}^2}{\hbar v |\Delta F|} \text{ s}^{-1} \qquad (4)$$

by multiplying the frequency at which the S–S bond moves through the crossing (i.e., the vibrational frequency 1.8×10^{13} s^{-1} of the S–S bond) times the LZ probability of a surface hop. Here v is the speed at which the S–S bond moves through the crossing point. We found that the dominant factor in determining the rate was the $H_{1,2}^2$ factor. So, using the fact that $H_{1,2}$ values of 300 cm^{-1} generated rates of 10^{12} s^{-1} from the LZ formula, we were able to propose a simple scaling formula
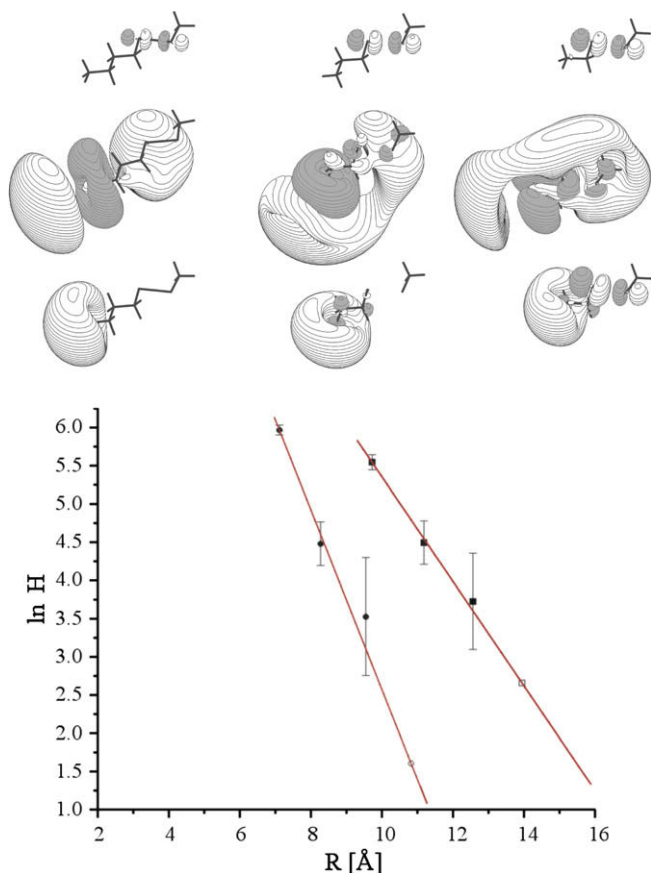
Fig. 5. Plots of ln $H_{1,2}$ (cm^{-1}) vs. distance R (Å) between the center of the SS bond and the center of charge of the 3s ground (left line) and 3p excited (right line) Rydberg orbitals for the $^+H_3N–(CH_2)_k–S–S–CH_3$ model compounds having $k = 1$, 2, and 3. Also shown (top) are the structures of the $^+H_3N–(CH_2)_k–S–S–CH_3$ model systems and their SS σ^* (top), 3p (middle), and 3s (bottom) Rydberg orbitals (appear as Figs. 2 and 4 in Ref. [25]).

$$Rate \approx 10^{12} \left[\frac{H_{1,2}\ (cm^{-1})}{300}\right]^2 s^{-1} \qquad (5)$$

to estimate the rates (for S–S bond cleavage) in terms of $H_{1,2}$ only.- Because the rates of relaxation from one Rydberg level to the next are ca. $10^6\ s^{-1}$, the findings just discussed allowed us to conclude that intra-peptide electron transfer from an excited Rydberg orbital to an SS σ^* orbital could be feasible (i.e., occur at rates exceeding the relaxation rates of $10^6\ s^{-1}$ which eventually lead to the ground Rydberg state, H or NH$_3$ loss, and termination of the opportunity for electron transfer) if

$$\left[\frac{H_{1,2}\ (cm^{-1})}{300}\right]^2 \gg 10^{-6}. \qquad (6)$$

This, in turn, requires that $H_{1,2}$ be greater than 0.3 cm^{-1}.

As the $H_{1,2}$ data shown in Fig. 4 suggest and results from additional work [44] support, the $H_{1,2}$ values for Rydberg levels having $n \geqslant 4$ are small (i.e., a few cm^{-1}), and can be expected (as we show later) to become even smaller as n increases. It is essentially impossible to compute ab initio adiabatic energy surfaces undergoing an avoided crossing to (relative) accuracies of a few cm^{-1}, let alone to the 0.3 cm^{-1} accuracy needed to determine the highest Rydberg principal quantum number that can yield inter-peptide electron transfer. This difficulty then convinced the author that an analytical expression for how the $H_{1,2}$ matrix elements should depend upon the n quantum number was needed, and this development [44] is what we will now discuss.
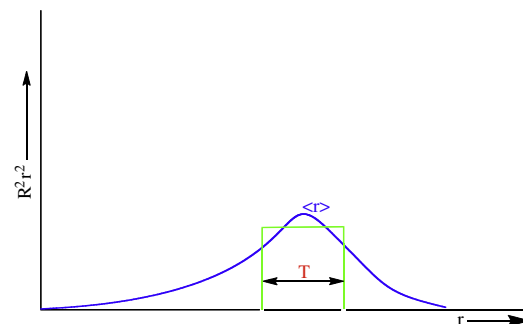
Fig. 6. Qualitative depiction (blue curve) of the radial probability density $|R|^2 r^2$ of a Rydberg orbital as a function of distance r from the positive center of the orbital to the electron. Also shown (green) is the radial shell characterized by the average radial size $\langle r \rangle$ and the thickness T of the orbital (taken from Ref. [45]).

2.5.2. An analytical expression for how $H_{1,2}$ depends on the Rydberg orbital's n quantum number

The analytical expressions obtained in Ref. [44] are based on a model in which

i. A Rydberg orbital's radial wave function is approximated in terms of its large-r hydrogenic form

$$R_n(r) = N r^{n-1} e^{-\frac{Zr}{na_0}}. \qquad (7)$$

This approximation ignores all of the (small-amplitude) radial oscillations that produce radial nodes at smaller distances. It also ignores the angular shape[6] of the Rydberg orbital. It represents the Rydberg orbital's radial probability density in terms of its largest-amplitude peak, which occurs at large-r.

ii. This representation of the radial probability density in terms of $r^2 R_n^2(r)$ is further approximated in terms of a radial 'shell' of uniform electron density centered at a distance $\langle r \rangle$ computed as the expectation value of r for the above $R_n(r)$ function:

$$\langle r \rangle = \frac{n(n+\frac{1}{2})a_0}{Z} \qquad (8)$$

(a_0 is the Bohr radius 0.529 Å) and having a thickness T

$$T = \sqrt{\langle r^2 \rangle - \langle r \rangle^2} = \frac{\sqrt{2n+1}}{2} \frac{na_0}{Z} \qquad (9)$$

evaluated as the mean-square width of the radial probability density $P(r) = r^2 |R_n(r)|^2$, where

$$\langle r^2 \rangle = \frac{(n+\frac{1}{2})(n+1)n^2 a_0^2}{Z^2}. \qquad (10)$$

In Fig. 6, we show qualitative representations of the Rydberg orbital's radial probability density (ignoring inner-region nodal character) and the shell used to model it.

To estimate the $H_{1,2}$ coupling strength between an SS σ^* or amide π^* orbital and a Rydberg orbital having quantum number n, we

(i) assumed that $H_{1,2}$ would be proportional to the overlap between the two orbitals,
(ii) approximated the wave function of the Rydberg orbital as being uniform within the shell of radius $\langle r \rangle$ and thickness T having volume V_n: $\psi_n(\mathbf{r}) = (1/V_n)^{1/2}$,

---

[6] Rydberg orbitals having different angular momentum (L) have different number of radial nodes and different angular shapes. In the approximation discussed here, we focus only on the regions of space where the Rydberg orbital has its highest probability density and we do so for what ever orbital (i.e., whatever L-value) is directed toward the SS σ^* or amide π^* orbital it is coupling with.

Table 1

Radial sizes and maximum electron transfer rates for transfer from Rydberg orbitals of various principal quantum number n to a valence SS σ^* or OCN π^* orbital.

Principal quantum number	Radial size[a] $\langle r \rangle$ (Å) for $Z = 1$	Thickness (Å) for $Z = 1$	Maximum rate[b] s^{-1} for $Z = 1$
3	5.5	2.1	10^{12}
4	9.5	3.2	2×10^{11}
5	14.5	4.4	7×10^{10}
6	20.6	5.7	3×10^{10}
7	27.8	7.2	1×10^{10}
8	36.0	8.7	6×10^{9}
10	55.5	12	2×10^{9}
20	217	34	4×10^{7}

[a] According to Eqs. (8) and (9), $\langle r \rangle$ and T should scale with Z as Z^{-1}.

[b] According to Eq. (11) and the fact that the rate depends on S^2, the rate should scale with Z as Z^3.

(iii) approximated the wave function of the SS σ^* or amide π^* orbital as being constant within a volume V_{bond} assumed to be small enough to be fully contained within the Rydberg orbital's shell: $\psi_{bond}(\mathbf{r}) = (1/V_{bond})^{1/2}$. The V_{bond} was expressed $4/3\pi(xa_0)^3$ in terms of a dimensionless variable x expected to be of the order of 5–10 (i.e., the valence orbitals are assumed to be smaller than the Rydberg orbitals and ca. 5–$10a_0$ in radial extent),

(iv) evaluated the overlap S by integrating the product of the two wave functions $\psi_n(\mathbf{r})$ and $\psi_{bond}(\mathbf{r})$ over the volume V_{bond} they share:

$$S = \int_{V_{bond}} \frac{1}{V_{bond}^{1/2}} \frac{1}{V_n^{1/2}} d^3r = \frac{V_{bond}^{1/2}}{V_n^{1/2}} = \sqrt{\frac{2x^3Z^3}{3n^3(n+\frac{1}{2})^2\sqrt{2n+1}}}. \quad (11)$$

This result then allowed us to estimate the rates for electron transfer from a Rydberg orbital with quantum number n to an SS σ^* or amide π^* orbital in terms of the rates we obtained earlier for transitions from $n = 3$ Rydberg orbitals to such an orbital (ca. 10^{12} s^{-1}) by assuming the rates will scale as the square of the overlap which gave:

$$Rate_n = \frac{3^3(3+1/2)^2\sqrt{2(3)+1}}{n^3(n+1/2)^2\sqrt{2n+1}} \times 10^{12} \text{ s}^{-1}. \quad (12)$$

In Table 1 we show how these rates and the size $\langle r \rangle$ of the Rydberg orbital vary with n.

Clearly, this model suggests that (i) electron transfer rates decay slowly with n and should exceed the rates of relaxation within the Rydberg state manifold for n values as high as 20 and (ii) electron transfer distances of over 100 Å may be possible. We will have more to say later about the implications these predictions have for understanding ECD or ETD bond cleavages.

However, first it is important to distinguish the two trends in electron transfer rates that we have been discussing, and we make use of Fig. 7 for this purpose.

In Fig. 5, we showed how the size of $H_{1,2}$ decays exponentially with the distance between the center of the Rydberg orbital and the center of the SS σ^* orbital (the same happens for the amide π^* orbital case). The basis for this trend is illustrated in the top left picture in Fig. 7 where we see how the overlap between the SS σ^* orbital and the Rydberg orbital decreases as the two are separated further and further from the shell of high density in the Rydberg orbital. This trend is characteristic of how the coupling (and hence the electron transfer rate) between a *given* Rydberg orbital and an SS σ^* or amide π^* orbital decays with distance.

The second trend relates to how the coupling (and rate) between an SS σ^* or amide π^* orbital and a Rydberg orbital varies

with the n quantum number of the Rydberg orbital assuming the SS σ^* or amide π^* orbital resides fully within the radial shell of the Rydberg orbital. It is this trend that is illustrated by the data shown in Table 1. The basis for this trend is shown in Fig. 7 through the progression of green SS σ^* orbitals overlapping with 3s, 4s, 4p, and 5s Rydberg orbitals with the σ^* orbital held at a distance $\langle r \rangle$ which allows it to be subsumed by the Rydberg orbital's shell of high electron density.

To understand the implications of these two trends, consider an SS σ^* or amide π^* orbital within a multiply positively charged polypeptide and assume the σ^* or π^* orbital experiences sufficient Coulomb stabilization to render it capable of exothermically attaching an electron. For a concrete example, think of the SS bond site shown in Fig. 1. Now, consider what can happen if an ECD, ETD, or ECID electron were to attach to one of the protonated amine sites in Fig. 1. If it attached to the nearby site residing $R_1 = 5$–10 Å away from the SS bond, Table 1 tells us an $n = 3$ or 4 Rydberg orbital will be most effective at transferring the electron to the SS σ^* orbital. Rydberg orbitals with higher-n will *not* be effective because the SS σ^* orbital will be too close to be within their radial shell of high electron density. If an electron attached instead to a more distant site residing $R_J = 15$–30 Å away from the SS bond, the $n = 5$, 6, and 7 Rydberg orbitals will be most effective. For Rydberg orbitals with higher-n, the SS σ^* orbital will be too close to be within their radial shell; for Rydberg orbitals with $n = 3$ or 4, the SS σ^* will be outside the shell (so the exponential decay of $H_{1,2}$ will render the Rydberg orbital ineffective).

It thus appears that electron transfer can occur, at rates (10^{10} s^{-1} or higher) much in excess of the relaxation rates (10^6 s^{-1}) within the Rydberg levels, from a positively charged site within 50 Å from the SS σ^* or amide π^* site as long as Rydberg levels having n up to 7 can be populated. This prediction suggests an experimental test:

(i) Using an anion donor (for ETD) that can populate, for example, only $n = 3$ and 4 Rydberg levels should limit electron transfer to ca. 10 Å. So, SS bond cleavage should not occur for the system shown in Fig. 2 (where 10, 15, or 20 Ala units appear in the helices and thus have positively charged Lys units 18, 24, and 32 Å from the SS bond).

(ii) Using an anion donor that can populate $n = 6$ and 7, transfer over 20–30 Å is expected, so SS bond cleavage should occur.

Of course, we know that ECD electrons, which presumably can populate higher-n Rydberg levels, do induce SS bond cleavage for the species in Fig. 2 even when there are 20 Ala units in the helices.

In addition to being consistent with what is found for ECD experiments on the quasi-linear model peptides in Fig. 2, this analysis also suggests why very high-n Rydberg levels (e.g., with $n > 10$) probably do not play a key role in typical analytical ECD, ETD, or ECID experiments on multiply charged polypeptides. First, in ECID, such n-values cannot be populated; likewise, in ETD unless the anion donor has a very low electron binding energy. However, even in ECD, which can populate high-n Rydberg levels,

(i) An orbital with $n > 10$ cannot effectively transfer an electron to a σ^* or π^* orbital that is *closer* than ca. 50 Å; the orbital is to close to reside within the shell of the Rydberg orbital.

(ii) Although an orbital with $n > 10$ can transfer an electron over 50 Å or more, the typical multiply positively charged polypeptide likely has another positive site much closer to the σ^* or π^* orbital; transfer from a lower-n Rydberg orbital on this closer positive site will have a higher rate and will thus dominate.

However, the last point just raised, that transfer from a lower-n Rydberg orbital on a closer site is likely more important, caused the
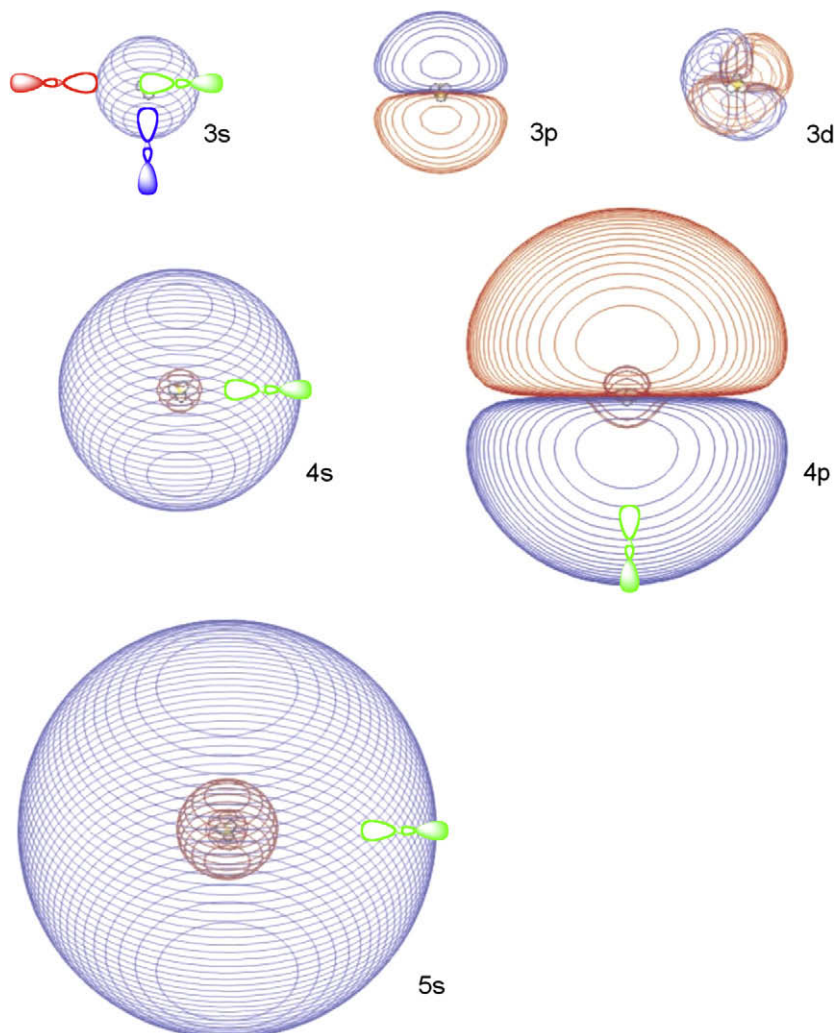
Fig. 7. Plots of 3s, 3p, 3d, 4s, and 5s Rydberg orbitals of NH_4 with the outermost contour containing 60% of the electron density of that orbital. Also shown are qualitative illustrations of SS σ^* orbitals at positions producing maximum (green), intermediate (blue), and low (red) overlap with some of the Rydberg orbitals (taken from Ref. [45]).

author to address another question. Does the electron have to arrive at this closer site in the initial ECD capture or ETC transfer event, or could it be transferred from a Rydberg orbital on another positively charged site? It is this issue that we now need to address.

2.6. Rydberg-to-Rydberg electron transfer

To consider the possibility of electron transfer from one Rydberg site to another, we carried out a series of calculations [25,28] on

  (i) A model system $[(NH_4)^+ \cdots (N(CH_3)_4)^+]$ (to represent a protonated amine and a fixed-charge site) with one electron attached; the electron could reside either on the ammonium or tetramethyl ammonium site, and

 (ii) a model system $[(N(CH_3)_4)^+ \cdots C(NH_2)_3^+]$ (to represent a fixed-charge site and an arginine side chain site) with one electron attached; the electron could reside either on the tetramethyl ammonium or arginine side chain site.

In Fig. 8 we plot the energies of several low-lying states for the latter system as functions of the distance between the two central atoms in the Rydberg sites. Note that the lowest-energy state, in which the electron resides largely on the $N(CH_3)_4^+$ site which has

a larger recombination energy than does the $C(NH_2)_3^+$ site, does not undergo an avoided crossing with any other state. However, the excited states do undergo avoided crossings. Although it is not possible to see with enough resolution in Fig. 8, the $H_{1,2}$ values associated with the avoided crossings found [25,28] for the $[(NH_4)\cdots(N(CH_3)_4)]^+$ and $[(N(CH_3)_4)\cdots C(NH_2)_3]^+$ model systems are comparable in size ($\geqslant 100\ cm^{-1}$) to those discussed earlier for Rydberg-to-valence electron transfer.

The primary conclusions of these studies [25,28] were that

  (i) An electron occupying an excited Rydberg state on one site can undergo transfer to a lower-energy (or equal-energy) Rydberg state on the other site.

 (ii) An electron occupying the ground Rydberg state on the site having higher electron binding energy *cannot* undergo transfer to a Rydberg state on a different site with lower binding energy.

(iii) An electron occupying the ground Rydberg state on a site having lower electron binding energy *can* undergo transfer to a Rydberg state on a different site with higher binding energy.

The bottom line is that transfer to lower- or equal-energy Rydberg orbitals is possible but transfer to higher-energy Rydberg states is not.
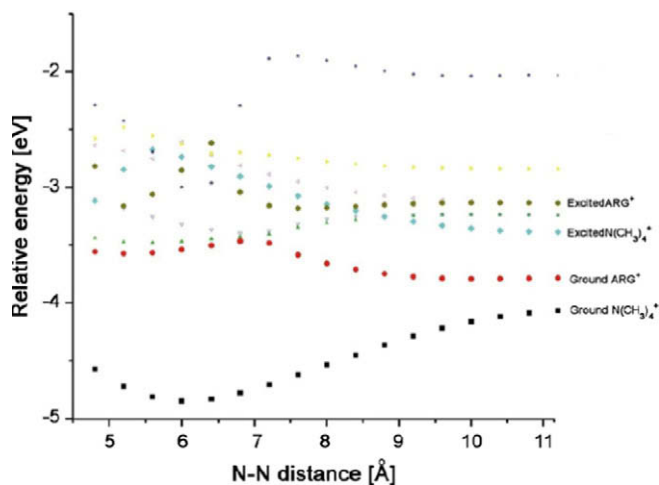
Fig. 8. Energies of ground and low-lying excited states of $[(N(CH_3)_4)\cdots C(NH_2)_3]^+$ as functions of the separation between the nitrogen atom of the trimethyl ammonium and the carbon atom of the arginine-type site (taken from Ref. [28]).
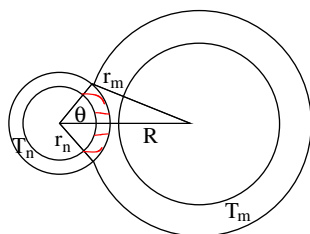
Fig. 9. Qualitative depiction of two s-symmetry Rydberg orbitals having sizes characterized by radii r_n and r_m with thicknesses T_n and T_m separated by a distance $R < r_n + r_m$.

However, as in the Rydberg-valence studies discussed earlier, we were only able to carry out ab initio calculations for model Rydberg systems having low principal quantum numbers (actually, only for $n = 3$). We therefore needed to devise a route to allow us to estimate the rates of Rydberg-to-Rydberg electron transfer between states with different n-values. To do so, we employed [44] the simple radial shell model of the Rydberg orbitals described earlier.

In Fig. 9, we show shell depictions of two Rydberg orbitals having radii $r_m \geqslant r_n$ and thicknesses $T_m \geqslant T_n$ and with a separation R between their centers. When $R = r_m + r_n$, the outermost part of each orbital's shell barely touches that of the other, and so there is no overlap between the two orbitals. Within the range of separations $r_m + r_n - T_n > R > r_m + r_n - T_n - T_m$ much volume of orbital n's shell will be inside the shell of orbital m, and the overlap will be largest when $R = r_m + r_n - T_n - T_m$.

The overlap integral S between the two approximate wave functions $\psi_n(\mathbf{r}) = (1/V_n)^{1/2}$ and $\psi_m(\mathbf{r}) = (1/V_m)^{1/2}$ can be evaluated as discussed earlier

$$S = \int_{\text{red}} \frac{1}{\sqrt{V_n}} \frac{1}{\sqrt{V_m}} = \frac{V_{\text{red}}}{\sqrt{V_n}\sqrt{V_m}}. \quad (13)$$

The volume of the region colored in red in Fig. 9 was shown in Ref. [44] to be

$$V_{\text{red}} = 2\pi r_n^2 T_n \frac{2Rr_n + r_m^2 - r_n^2 - R^2}{2Rr_n}. \quad (14)$$

When evaluated at $R = r_n + r_m - T_n - T_m$, the distance at which maximum overlap of the shells is expected, V_{red} reduces to

$$V_{\text{red}} = \frac{2\pi r_n T_n (T_m + T_n)}{1 + \frac{r_n}{r_m}}$$

$$= \pi \left(\frac{a_0}{Z}\right)^3 \frac{n^2(n + 1/2)^{3/2}(m(m + 1/2)^{1/2} + n(n + 1/2))}{1 + \frac{n(n+1/2)}{m(m+1/2)}}, \quad (15)$$

where the second identity arises from substituting the expressions for the sizes ($r_n = \langle r \rangle_n$ and $r_m = \langle r \rangle_m$) and for the thickness factors T_n and T_m given earlier. These results in turn allowed the square of the overlap integral between the two Rydberg orbitals to be expressed as

$$S_{n,m}^2 = \frac{n\sqrt{n+1/2}}{8m\sqrt{m+1/2}} \frac{1}{m+1/2} \left[\frac{1 + \frac{n\sqrt{n+1/2}}{m\sqrt{m+1/2}}}{1 + \frac{n(n+1)}{m(m+1)}}\right]^2. \quad (16)$$

Assuming that the electron transfer rates scale as $H_{1,2}^2$ and that $H_{1,2}$ is proportional to the overlap, we approximated the rate of transfer from a Rydberg orbital having quantum number m to another with quantum number n separated by a distance where their radial shells achieve maximum overlap as

$$Rate_{m \to n} = Rate_{3 \to 3} \frac{n\sqrt{n+1/2}}{m\sqrt{m+1/2}} \frac{3+1/2}{m+1/2} \left[\frac{1 + \frac{n\sqrt{n+1/2}}{m\sqrt{m+1/2}}}{1 + \frac{n(n+1)}{m(m+1)}}\right]^2. \quad (17)$$

This result suggests that

(i) Transfer rates between Rydberg orbitals having the same quantum number should decrease (slowly) with m as $Rate_{m \to m} \propto \frac{3+1/2}{m+1/2}$ and

(ii) Transfer rates between Rydberg orbitals with different quantum number n and $m > n$ should decrease as m increases as $Rate_{m \to n} \propto \frac{n\sqrt{n+1/2}}{m(m+1/2)^{3/2}}$.

(iii) The distance R between the two Rydberg sites determines, through $R = 2r_m - 2T_m$, the quantum number of the Rydberg orbital that will be most effective in causing the transfer.

So, the fastest transfer rates are expected for transfer between pairs of Rydberg orbitals having the same quantum numbers, and these rates should decrease slowly as that quantum number grows.

There is some experimental evidence is support of our prediction that transfer from one Rydberg site to another can occur if the transfer is to a lower- or equal-energy orbital, but we are unaware of any evidence in support of or against the predictions for how these transfer rates depend on the n quantum number.

The McLuckey group [9] performed a series of ETD experiments on triply charged peptides containing a disulfide linkage such as shown in Fig. 10a and b and denoted Ala–Gly–Cys(–Lys)–Cys–Ser–Thr–Phe–Thr. The amine sites on the Ala, Lys, and terminal Thr sites are protonated in the ion shown in Fig. 10a where their distances[7] to the disulfide linkage are also shown. In the ion shown in Fig. 10b, these three sites have been transformed into fixed-charge sites by chemically adding a unit denoted TMAB to the nitrogen of their amines (replacing one hydrogen of an amine group by the $-C=O-(CH_2)_3-N(CH_3)_3^+$ group). Of course, because of the size of the TMAB group, the distances to the disulfide unit are considerably larger in the second compound. In these experiments, compounds in which one or two of the sites are protonated and two or one have fixed charge were also examined. In Ref. [9] it was noted that the recombination energy for the protonated amine site is considerably higher than that of the fixed-charge $-N(CH_3)_3^+$ site, and both are lar-

---

[7] The geometries shown in Fig. 10 represent those of the minimum-energy structures found using a PM3 force field.

a

Ala-Gly-Cys-Lys
Thr-Phe-Thr-Ser-Cys } + 3 H

8.782 [Å]
Lys site

6.230 [Å]
Thr site

5.024 [Å]
Ala site

b

Ala-Gly-Cys-Lys
Thr-Phe-Thr-Ser-Cys } + 3 TMAB

12.108 [Å]
Lys site

10.199 [Å]
Thr site

5.422 [Å]
Ala site
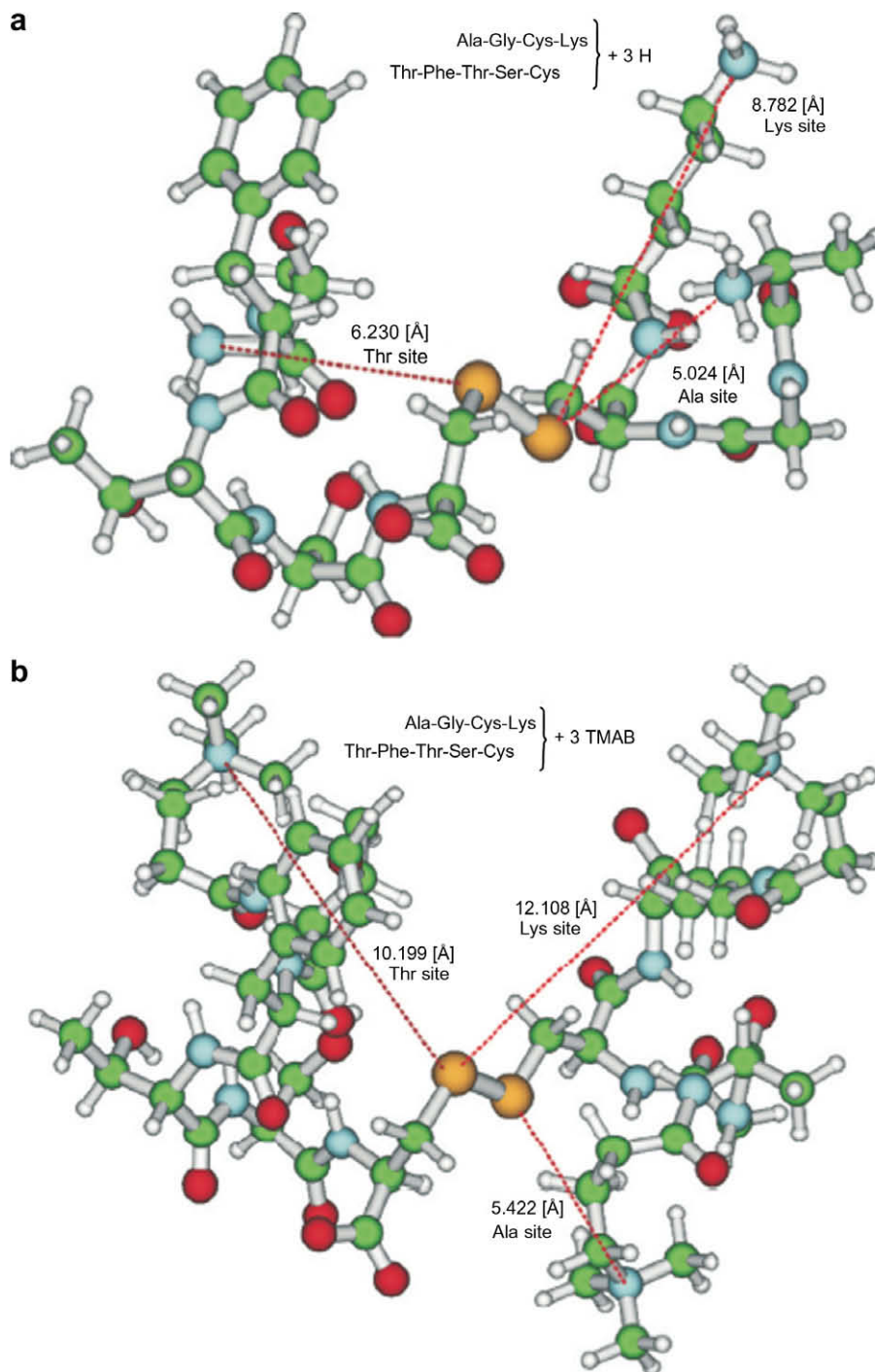
Fig. 10. Triply charged ions containing disulfide bond at the core with three arms whose termini can be protonated (a) or fixed-charged by adding TMAB to the Ala, Lys, and terminal Thr amines (b) (taken from Ref. 25).

ger than the electron binding energy (ca. 0.5 eV) of the azobenzene anion that served as the ETD donor.

All of the multiply charged cations shown in Fig. 10 have a disulfide-linked core and three 'arms' (Lys, Thr, and Ala) on whose termini the positively charged groups reside. When an arm has been modified by TMAB, it is longer than when unmodified. Even in the compound with three long arms (Fig. 10b), the charged sites are close enough to the S–S bond to render it amenable to exothermic direct electron attachment. It is important to notice that, when TMAB-substituted, the distances between the positive sites and the

disulfide linkage increase considerably more for the Lys and Thr arms than for the Ala arm (compare distances in Fig. 10a and b).

The ETD experiments of Ref. [9] using azobenzene anion[8] as the electron donor showed 71% disulfide cleavage for the species shown

---

[8] The size of this anion, combined with the fact that the disulfide bond in the species shown in Fig. 10 appears to be quite shielded by the surrounding arms, suggests that direct electron transfer the SS σ^* orbital would be even less likely than the 1–10% predicted in our earlier work. In other words, we expect that the ETD electron will initially attach to a positively charged site.

in Fig. 10a and 80% disulfide cleavage for that shown in Fig. 10b. Moreover, when only one of the protonated amine sites in Fig. 10a was chemically modified by TMBA, disulfide cleavage still accounted for 68% of the ETD bond cleavage products[9]. So, the percent of disulfide cleavage ranged from 68 to 80 % for species for species containing *zero, one or three* TMAB substitutions. In contrast, the species containing *two* TMAB substitutions produced only 36% disulfide cleavage. In the latter compound, there are two long arms and one short arm, but, as noted in Ref. [9], synthetic limitations precluded knowing where the TMAB substitutions exist (except, of course, when all three arms are substituted).

In Ref. [25], we make a postulate that rationalized the puzzle just noted in relation to why the species with two TMAB substitutions behaves differently as we now explain. First note in Fig. 10 that, when the Ala site is TMAB-substituted, the distance of its terminus to the S–S bond is only slightly increased compared to when it is protonated. In addition, adding the TMAB substitution to the Ala site makes little change in the internal Coulomb repulsion energy of the triply charged peptide, In contrast, TMAB substituting the Lys or Thr sites moves their termini much further from the SS bond and from the other charged sites. We thus postulated in Ref. [25] that, in the synthetic reactions used to carry out the TMAB substitutions, the first and second TMAB substitutions occur at the Lys and Thr sites. Adding TMAB to either of these sites substantially increases the average arm length and thus substantially decreases the Coulomb repulsions within the peptide, thus making the products more thermodynamically stable. This postulate implies that in the triply, doubly, and singly protonated species, the Ala site remains protonated; only when all three sites have been TMAB-substituted is the Ala site converted to fixed charge.

Based on this postulate and making use of the predictions about Rydberg-to-Rydberg electron transfer discussed earlier, we were able to rationalize the exceptional behavior of the species having two TMAB substitutions as follows:

(i) For the species in Fig. 10 having *three or zero* protonated sites, the attached electron can migrate from charged site to charged site because all three sites are essentially identical once it ends up on the Ala site, which is only ca. 5 Å from the S–S bond with or without TMAB substitution, it can undergo transfer to the S–S σ^* orbital thus giving disulfide cleavage.

(ii) For the species having *one* protonated site (by assumption, Ala), the electron might attach to the close (Ala) after which it can undergo transfer to the S–S bond, or it might attach to the Lys or Thr. However, an electron attached to TMAB-substituted Lys or Thr cannot subsequently transfer to the Ala site; it is endothermic to do so. Moreover, because the substituted Lys and Thr termini are quite far from the SS bond, electron transfer from them to the SS bond will be slower than from Ala to the SS bond. Hence, for the species with one protonated site, we expect the rate of SS cleavage to be low and to be dominated by events in which the electron is initially captured at the Ala site; this prediction is in line with the 36% SS bond cleavage observed for such species.

(iii) For the species having *two* protonated sites, our assumption requires one of these to be the Ala site. In the electron initially attaches to the (protonated) Ala site or to the other protonated site, it can, respectively, (a) be transferred directly to the nearby SS bond or (b) undergo Rydberg-to-Rydberg transfer to the Ala site and subsequently transfer

to the SS bond. Only that fraction of initial electron attachment to the TMAB-substituted site will be severely limited (because of the large distance from this site to the SS bond) in cleaving the SS bond. So, species with two protonated sites should show SS bond cleavage yields higher than for species with one protonated site but less than for species with three or zero protonated sites.

This evidence is, to date, the strongest in support of the claim that Rydberg-to-Rydberg electron transfer can occur. Yet, as the reader no doubt detects, the evidence is not conclusive and relies on assumptions about which sites remain protonated and which are TMAB-substituted. Clearly, there is need for more focused and definitive experiments to better address this issue. Before closing this discussion, two other suggestions regarding the role of Rydberg states deserve to be mentioned. First, as mentioned earlier, computational evidence was presented in Ref. [30] suggesting that Rydberg states that are delocalized over two or more positively charged sites might be formed and thus might be operative in ECD/ETD. This evidence is consistent with the model we offered here in which Rydberg orbitals on different sites interact with one another. Secondly, in one of the earlier contributions from the McLafferty lab on ECD [2], it was mentioned that Prof. John Brauman had suggested, knowing that such states can be long-lived (see Footnote 23 in Ref. [2]) that electron capture into a high-n Rydberg state could be an important step in the ECD mechanism. This author surmises that Prof. Brauman also believed the large radial extent of such an orbital would allow it to transfer its electron over a long distance. As it turns out (if our model is valid), the Brauman prediction was very much on the money although our model suggests (i) that *very* high-n Rydberg levels are probably not key, rather, those having $n < 10$ or 20 probably are; and (ii) that the key Rydberg levels will be those whose radial extent closely matches (but does not exceed) the distance to the SS or N–C$_\alpha$ bond to be cleaved.

3. Present status

At present, the evidence discussed above leads us to think that the following events occur when an ECD, ETD, or ECID electron induces SS or N–C$_\alpha$ bond cleavages within multiply positively charged gas-phase polypeptides:

1. Initial electron attachment [17,18,22] most likely (90–99%) takes place into a Rydberg orbital located on one of the peptide's positive sites, although in a small (1–10%) fraction of the attachment events, the electron can attach directly into SS σ^* or amide π^* orbital. However, such direct orbital attachment can take place only when the orbital is close enough to positive sites to experience sufficient (ca. 1 eV for SS and 2.5 eV for amide) Coulomb stabilization.
2. ECD can populate very high Rydberg levels, while energy constraints limit ETD and ECID to lower Rydberg levels. However, the fact that ECD, ETD, and ECID fragmentation patterns and yields are quite similar suggests that, even in ECD, substantial relaxation to lower Rydberg levels occurs prior to the rate-determining steps for bond rupture.
3. Attachment into any excited Rydberg orbital on a positive site is followed by
   a. a cascade of radiationless or radiative relaxation events to lower-energy Rydberg levels on time scales of ca. 10^{-6} s per transition [45], during which
   b. electron transfer from an excited Rydberg orbital to an SS σ^* or amide π^* orbital can take place at rates exceeding 10^6 s^{-1} even for Rydberg orbitals having principal quantum

---

[9] In all of these experiments, other outcomes took place but with low branching ratios, proton transfer to the azobenzene anion and electron transfer to the parent ion with no fragmentation taking place being the two most common.

numbers as high as 20. However, only SS σ^* or amide π^* orbitals that experience Coulomb stabilization exceeding 1 eV or 2.5 eV, respectively, can act as electron acceptors in such transfers.

4. Once a ground 3s Rydberg orbital is occupied on a protonated amine site, prompt (ca. 10^{-9} s) H-atom loss ($R–NH_3 \rightarrow RNH_2 + H$) or NH_3 loss occurs, which thus terminates the possibility of electron transfer from this site to an SS or N–C_α site.

5. The only excited Rydberg orbitals that can transfer electrons to SS or amide bonds are those that have

   a. $n <$ ca. 20 (so that the electron transfer rate exceeds 10^6 s^{-1}),

   b. radial size $\langle r \rangle = n(n + 1/2)a_0/Z$ (see Table 1) close to their distance to the SS or amide bond site so that Rydberg-valence orbital overlap is favorable (if n is too small, the Rydberg orbital does not extend far enough; if n is too large, the valence orbital is too close and thus does not overlap the radial shell of the Rydberg orbital), and

   c. vertical (i.e., near the equilibrium geometry of the parent ion) electron binding energies very similar to the vertical binding energy of the SS σ^*- or amide π^*-attached state (so that the Rydberg-valence state curve crossing occurs near the parent's equilibrium geometry).

6. It is also possible for an electron initially attached into an excited Rydberg orbital on one positive site to undergo transfer [25–28] to a Rydberg orbital (having similar or higher electron binding energy) on another positive site. However, transfer to an orbital with a lower electron binding energy cannot occur. Such processes allow attached electrons to migrate throughout the polypeptide. The rates of such Rydberg-to-Rydberg transfers are expected to be largest when the principal quantum numbers of the two Rydberg orbitals are the same and to decrease slowly as the principal quantum numbers of the Rydberg orbitals grow. The Rydberg orbitals most effective in causing the transfer have quantum numbers determined by $R = 2r_m - T_m$, where R is the distance between the two sites and r_m and T_m are the radial size and thickness of the optimal Rydberg orbital.

4. Future challenges

There remain significant challenges on both the experimental and theoretical fronts when it comes to testing the hypotheses and predictions of the mechanisms we and others have put forth. In terms of experiments, it would be very useful to design and carry out ECD, ETD, or ECID fragmentation studies on species in which

(i) the geometry of the parent ion (at least the distances among SS σ^*, amide π^*, and charged sites) is constrained (e.g., by using rigid frameworks) so one can be confident in estimating the Coulomb stabilization energies and thus the electron binding energies of the various sites,

(ii) the Rydberg level into which an electron is initially attached can be systematically varied (or at least systematically limited),

(iii) the distance from the Rydberg site of initial electron attachment and the bond site (SS σ^*, amide π^*) or other Rydberg site to which electron transfer occurs is systematically varied.

The first issue (geometrical constraint) could be addressed by using rigid 'spacer' units such as the $(Ala)_k$ helices shown in Fig. 2 or saturated cyclic groups such as shown in Fig. 11.

To constrain the Rydberg level into which initial electron attachment occurs, several options may exist. Certainly, one could employ ETD anion donors having a range of electron binding energies; energy conservation would then limit the highest Rydberg le-
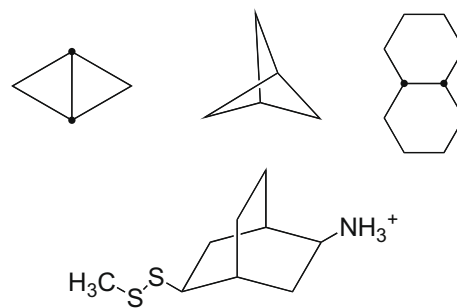
Fig. 11. Potential rigid spacer groups used to constrain distances among bond and charged sites with one example of such sites shown to illustrate.
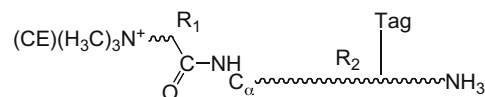
Fig. 12. Qualitative depiction of parent ion containing two charged groups of different electron binding strength, an N–C_α bond, and an electron scavenging tag.

vel that could be populated. However, it would be optimal if these anions could not differ too much in their steric 'bulk' so one could be reasonably certain that differences in observed fragmentation patterns resulted primarily from differences in the donor electron binding energies. One could also vary the nature of the positively charged sites to vary their electron binding strengths and thus the energies and radial sizes of their Rydberg states. For example, the Aarhus group [46] used $-NH_3^+$, $-N(CH_3)_3^+$, $-NH_3^+(CE)$, and $-N(CH_3)_3^+(CE)$ as charged sites, where CE indicates that the cation site is encapsulated within a crown ether thus reducing its electron binding strength. For these four positive groups, the electron binding strengths are 4.3, 3.1, 2.1, and 2.3 eV, respectively. In addition, one could use state-selected Rydberg levels of atoms (e.g., selected by laser excitation) to transfer an electron to the parent peptide as the groups of Profs. Schermann and Desfancois and of Prof. Compton [47,48] do when they form dipole-bound anions. This approach would allow one to best control which Rydberg level is initially populated because the workers in Refs. [47,48] have shown that electron transfer occurs primarily when the energy level of the Rydberg atom matches very closely that of the electron acceptor.

Clearly, the distances between various (SS σ^*, amide π^*, and positive) sites should be systematically varied to gain information about the dependences on Rydberg principal quantum number offered here. For example, one could

(i) locate a positive site of low electron binding energy (e.g., $-N(CH_3)_3^+$ encapsulated in a crown ether) close enough (R_1 in Fig. 12) to render an amide π^* orbital amenable to exothermic electron attachment,

(ii) attach another positive site of higher binding energy (e.g., the $-NH_3^+$ site in Fig. 12) a fixed (by using a rigid framework as above) distance R_2 from the amide unit,

(iii) use an ETD donor that can populate (at least a few) states of the $-NH_3^+$ site but none of the other site, and

(iv) vary the distance R_2.

Another tool that could be used in experimental studies is the tagging technique used by the Beauchamp group [49]. In this approach, the side chain of one or more amino acids is replaced by a functional group of significant electron affinity. In Ref. [49] it was demonstrated that the EA of the tag had no influence on the rate of electron capture by the parent ion, which lends further sup-

port to the idea that the electron is initially attached to one of the positive sites. It was also shown that tags with high EAs can 'intercept' electron transfer (from a Rydberg orbital to a bond site) and thus inhibit backbone bond cleavage.

Of course, there is also remaining to be done on the theoretical front.

(i) Most of this author's work on electron transfer from Rydberg orbitals to valence orbitals has been limited to SS σ^* orbitals as the electron acceptor. Although there are good reasons to believe that many of the conclusions drawn from that work also apply when an amide π^* orbital is the acceptor, this case really should be more fully examined.

(ii) The simple spherical shell model used to describe the Rydberg orbitals needs to be tested by carrying out evaluations of the overlaps between valence (e.g., SS σ^* and amide π^*) orbitals and real (i.e., analytical functions of r, q, and f) Rydberg orbitals having principal quantum numbers in the range $3 \leqslant n \leqslant 20$. The purpose is to see if there are any 'surprises' that the simple model does not at least qualitatively account for.

(iii) The model systems that we and others have been able to address have been limited to rather small cations representative of mono-, di-, and tri-peptides. Clearly, there is need to extend these studies to larger systems so that the effects of multiple charging and of how the charges are distributed (i.e., spread out among the side chains or more localized) within the polypeptide can be addressed. Although such studies will require considerably greater computational resources, it is our belief that what has been learned from work on smaller systems will offer much guidance thus rendering them feasible.

(iv) We need to find a way to estimate the relative rates of Rydberg-to-valence and Rydberg-to-Rydberg electron transfer so we can better suggest whether an electron attached to a positive site is more likely to migrate to an SS or amide bond or to another positive site. Although the analytical approximations described earlier allow us to make predictions about how the Rydberg-to-valence rates will depend on the Rydberg orbital's n quantum number and analogously for the Rydberg-to-Rydberg rates, we do not yet have a firm grasp on how to predict the relative rates of these two events. In addition to coming up with a new theoretical approach, it would be beneficial to design experiments (e.g., by competitive kinetics) that could directly probe the relative sizes of these rates.

(v) The analytical approximations discussed here allow us to make predictions about how the Rydberg-to-valence rates will depend on the Rydberg orbital's n quantum number, but we also need to carry out an analysis (or extensive computational studies) of how these rates depend upon the electron binding strength of the valence orbital. This knowledge is important for understanding the relative rates of transfer to SS σ^* and amide π^* orbitals and to orbitals on molecular tags.

Finally, it is natural to ask to what extent the phenomena discussed here will arise when positively charged polypeptides or proteins in solution (in vivo or in vitro) encounter a reagent that might transfer an electron to them. We offer these speculations because, in a recent Frontiers Article [50], Leon Sanche did an excellent job explaining how electron attachment to DNA and related molecules can induce new chemistry under a wide variety of environments. First, because each positive site of the polypeptide is likely to be either (i) hydrogen bonded to a nearby site in the same ion or (ii) strongly solvated by the surrounding medium, it is unlikely that the manifold of Rydberg states associated with the posi-

tive sites will play a key role. It is thought that Rydberg orbitals disappear (i.e., become pushed to much higher energy) when a positive site is completely or primarily surrounded by several shells of solvent molecules. However, it is still possible that SS σ^* and amide π^* orbitals can be Coulomb stabilized by the positive charges in the polypeptide (and from any neighboring cations), although the Coulomb potential will be screened by the dielectric constant of the surrounding medium. Moreover, the anions formed upon cleavage of SS or N–C$_\alpha$ bonds will be stabilized by the surrounding solvent. Thus, one might expect to see some direct electron attachment to SS σ^* and amide π^* orbitals and the associated SS and N–C$_\alpha$ bond cleavage, but probably only close to positively charged sites because of the dielectric screening of the stabilizing Coulomb potential.

To conclude this Letter, the author would like to quote what Walter Cronkite famously said, 'and, that's the way it is', but, given the remaining uncertainty and the large amount of work that remains to be done, it is safer to say 'and, that's the way we think it is'.

Acknowledgments

References

[1] R.A. Zubarev, N.L. Kelleher, F.W. McLafferty, J. Am. Chem. Soc. 120 (1998) 3265.
[2] R.A. Zubarev, N.A. Kruger, E.K. Fridriksson, M.A. Lewis, D.M. Horn, B.K. Carpenter, F.W. McLafferty, J. Am. Chem. Soc. 121 (1999) 2857.
[3] R.A. Zubarev et al., Anal. Chem. 72 (2000) 563.
[4] R.A. Zubarev, K.F. Haselmann, B. Budnik, F. Kjeldsen, R. Jensen, Eur. J. Mass Spectrom. 8 (2002) 337.
[5] J.E.P. Syka, J.J. Coon, M.J. Schroeder, J. Shabanowitz, D.F. Hunt, Proc. Natl. Acad. Sci. 101 (2004) 9528.
[6] J.J. Coon, J.E.P. Syka, J.C. Schwartz, J. Shabanowitz, D.F. Hunt, Int. J. Mass Spectrom. 236 (2004) 33.
[7] S.J. Pitteri, P.A. Chrisman, S.A. McLuckey, Anal. Chem. 77 (2005) 5662.
[8] H.P. Gunawardena, M. He, P.A. Chrisman, S.J. Pitteri, J.M. Hogan, B.D.M. Hodges, S.A. McLuckey, J. Am. Chem. Soc. 127 (2005) 12627.
[9] H.P. Gunawardena, L. Gorenstein, D.E. Erickson, Y. Xia, S.A. McLuckey, Int. J. Mass. Spectrom. 265 (2007) 130.
[10] E.A. Syrstad, F. Turecek, J. Phys. Chem. A 105 (2001) 11144.
[11] F. Turecek, E.A. Syrstad, J. Am. Chem. Soc. 125 (2003) 3353.
[12] F. Turecek, M. Polasek, A. Frank, M. Sadilek, J. Am. Chem. Soc. 122 (2000) 2361.
[13] E.A. Syrstad, D.D. Stephens, F. Turecek, J. Phys. Chem. A 107 (2003) 115.
[14] F. Turecek, J. Am. Chem. Soc. 125 (2003) 5954.
[15] E.A. Syrstad, F. Turecek, Am. Soc. Mass. Spectrom. 16 (2005) 208.
[16] E. Uggerud, Int. J. Mass Spectrom. 234 (2004) 45.
[17] I. Anusiewicz, J. Berdys-Kochanska, J. Simons, J. Phys. Chem. A 109 (2005) 5801.
[18] I. Anusiewicz, J. Berdys-Kochanska, P. Skurski, J. Simons, J. Phys. Chem. A110 (2006) 1261.
[19] A. Sawicka, P. Skurski, R.R. Hudgins, J. Simons, J. Phys. Chem. B107 (2003) 13505.
[20] M. Sobczyk, P. Skurski, J. Simons, Adv. Quantum Chem. 48 (2005) 239.
[21] A. Sawicka, J. Berdys-Kochaska, P. Skurski, J. Simons, Int. J. Quantum Chem. 102 (2005) 838.
[22] I. Anusiewicz, J. Berdys, M. Sobczyk, A. Sawicka, P. Skurski, J. Simons, J. Phys. Chem. A109 (2005) 250.
[23] V. Bakken, T. Helgaker, E. Uggerud, Eur. J. Mass Spectrom. 10 (2004) 625.
[24] P. Skurski, M. Sobczyk, J. Jakowski, J. Simons, Int. J. Mass. Spectrom. 265 (2007) 197.

[25] M. Sobczyk, D. Neff, J. Simons, Int. J. Mass Spectrom. 269 (2008) 149.
[26] M. Sobczyk, J. Simons, Int. J. Mass. Spectrom. 253 (2006) 274.
[27] M. Sobczyk, J. Simons, J. Phys. Chem. B 110 (2006) 7519.
[28] D. Neff, M. Sobczyk, J. Simons, Int. J. Mass Spectrom. 276 (2008) 91.
[29] D. Neff, J. Simons, Int. J. Mass Spectrom. 277 (2008) 166.
[30] F. Turecek, X. Chen, C. Hao, J. Am. Chem. Soc. 130 (2008) 8818.
[31] X. Chen, F. Turecek, J. Am. Chem. Soc. 128 (2006) 12520.
[32] A.I.S. Holm et al., Int. J. Mass Spectrom. 276 (2008) 116.
[33] J. Chamot-Rooke, C. Malosse, G. Frison, F. Tureček, J. Am. Assoc. Mass Spectrom. 18 (2007) 2146.
[34] Y.M.E. Fung, T.-W.D. Chan, J. Am. Assoc. Mass Spectrom. 16 (2005) 1523.
[35] H. Konishi, Y. Yokotake, T.J. Ishibahsia, Mass Spectrom. Soc. Jpn. 50 (2002) 229.
[36] A.I.S. Holm et al., J. Phys. Chem. A 111 (2007) 9641.
[37] R. Hudgins, K. Håkansson, J.P. Quinn, C.L. Hendrickson, A.G. Marshall, in: Proceedings of the 50th ASMS Conference on Mass Spectrometry and Allied Topics, Orlando, Florida, June 2–6, 2002, A020420.
[38] G. Frison, G. van der Rest, F. Turecek, T. Besson, J. Lemaire, P. Matre, J. Chamot-Rooke, J. Am. Chem. Soc. 130 (2008) 14916.
[39] C. Dezarnaud-Dandine, F. Bournel, M. Troncy, D. Jones, A. Modelli, J. Phys. B: At. Mol. Opt. Phys. 31 (1998) L497.
[40] M. Seydou, A. Modelli, B. Lucas, K. Konate, C. Desfrancois, J.P. Schermann, Eur. Phys. J. D 35 (2005) 199.
[41] L.-S. Wang, X.-B. Wang, J. Phys. Chem. A 104 (2000) 1978.
[42] D. Neff, S. Smuczynska, J. Simons, Int. J. Mass Spectrom. 283 (2009) 122.
[43] A.I.S. Holm et al., J. Phys. Chem. A 111 (2007) 9641.
[44] D. Neff, J. Simons, J. Phys. Chem. A, in press.
[45] See Ref. [10] as well as F. Turecek, P. Reid, J. Int. J. Mass Spectrom. 222 (2003) 49.
[46] C. Skinnerup Jensen, A.I.S. Holm, H. Zettergren, J.B. Overgaard, P. Hvelplund, S. Brøndsted Nielsen, Am. Soc. Mass Spectrom. 20 (2009) 1881.
[47] S. Carles, C. Desfrancois, J.P. Schermann, D.M.A. Smith, L. Adamowicz, J. Chem. Phys. 112 (2000) 3726.
[48] H.S. Carman Jr., C.E. Klots, R.N. Compton, in: J.A. Kaye (Ed.), Isotope Effects in Gas-Phase Chemistry, ACS Symposium Series, vol. 502, American Chemical Society, Washington, DC, 1992, p. 181.
[49] C.H. Sohn, C.K. Chung, S. Yin, P. Ramachandran, J.A. Loo, J.L. Beauchamp, J. Am. Chem. Soc. 131 (2009) 5444.
[50] L. Sanche, Chem. Phys. Lett. 474 (2009) 1.

Jack Simons was born and reared in Girard, Ohio. He earned his B.S. degree in chemistry at Case Institute of Technology in 1967, his Ph.D. degree in chemistry at the University of Wisconsin in 1971, and held an NSF Postdoctoral position at MIT during 1970-1971. In 1971, he joined the faculty of the University of Utah where he currently holds the position of Henry Eyring Scientist and Professor.